First-principles determination of the Ni-Al phase diagram

1992 J. Phys.: Condens. Matter 4 945

(http://iopscience.iop.org/0953-8984/4/4/005)

J. Phys.: Condens. Matter 4 (1992) 945–959. Printed in the UK

First-principles determination of the Ni–Al phase diagram

A Pasturel†, C Colinet†, A T Paxton‡ and M van Schilfgaarde‡
† LTPCM, CNRS Unité de Recherche Associé 29, ENSEEG, BP 75, 38402 St Martin d'Hères Cédex, France
‡ SRI International, Menlo Park, CA 94025, USA

Received 16 July 1991, in final form 9 October 1991

Abstract. Phase stability in the Ni–Al binary system is investigated using linear muffin-tin orbitals total energy (LMTO) calculations. They provide total energies for the different existing compounds and, using Connolly–Williams inversion, the many-body interactions occurring in the FCC and BCC lattices. These interactions are used in conjunction with the Cluster Variation Method (CVM) to calculate the phase diagram. The computed phase diagram agrees very well with the experimental one.

1. Introduction

The modern theory of phase diagram calculations has been made possible by great advances in band-structure calculations, the theories of the configurational thermodynamics and phase transformations. Total energy calculations based on the local density approximation (LDA) are now sufficiently accurate to explain many properties of materials in terms of the underlying electronic structure [1]. An accurate calculation of the configurational free energy of the alloy is possible within various approximations such as mean field methods (Cluster Variation Method, CVM) or by numerical methods (Monte Carlo simulations) [2, 3]. In these models, it is assumed that the internal energy can be written as a sum of multi-site interactions which converge rapidly. The fact that these interactions can be derived from first-principle calculations establishes the basis of a comprehensive first-principles theory of cohesive, structural and thermodynamical properties of metals and alloys. Two extreme types of approach to the calculation of these interactions have been developed; the first one starts from the energy of the completely disordered solid solution calculated by the coherent potential approximation (CPA) [4]. The effective cluster interactions are calculated by the Embedded Cluster Method [5] or by the Generalized Perturbation Method (GPM) [6] using a perturbative treatment about the completely disordered state. In this case, the ordering energies can be written as an expression in terms of concentration-dependent nth-order effective cluster interactions. GPM can be developed with the first-principles multiple scattering formalism of the Korringa–Kohn–Rostoker coherent potential approximation [7]; however, to our knowledge, no phase diagrams have yet been provided by this approach although, in the framework of the tight-binding approximation, interesting results have been obtained [8–10].

0953-8984/92/040945 + 15 $04.50

The second approach is the so-called Connolly–Williams inversion [11] and the closely related ε–G approach [12]; here, the total energy is assumed to be written as a sum of configuration independent many-body interaction potentials multiplied by the multi-site correlation functions. The sum runs over all the cluster types and, in practice, it requires the existence of a maximum cluster beyond which the many body interactions are supposed to be negligible. This procedure has been used successfully by several authors [13–15] and we will adopt it here. The Ni–Al system presents both theoretical and technological interest, the aluminides having many desirable properties such as low density, high melting temperatures and high yield strength.

From a theoretical point of view, Sigli and Sanchez [16] have shown that a CVM treatment using effective pair interactions determined from available thermochemical data was able to give a good representation of the phase diagram. Several quantitative total energy calculations [17–20] have also been performed for ordered AlNi compounds using linearized methods [21]. All these calculations conclude that a strong hybridization between the p states of Al and the d states of Ni leads to the formation of bonding and antibonding states well separated by a pseudogap in the electronic density of states. The same trend has also been found using Tight Binding arguments [22]. A few calculations have treated more subtle effects such as the relative stabilities in Ni_3Al compounds [18]; van Schilfgaarde *et al* [23] have shown that non-self-consistent total energy calculations can be applied to this problem: they employ the linear muffin-tin method [21] using two different approaches. In the first approach, within the atomic sphere approximation, they employ an analogue of the local force theorem [24, 25], in which the total energy difference between two structures comprises the band-structure energy plus small Coulomb corrections. In the second approach, they make no shape approximations to the potential and employ a recasting of the local-density functional proposed by Harris and Foulkes [26]. All these results are in good agreement with experimental determinations of the energies of formation of Ni–Al comounds [27], which is the primary condition for the phase diagram determination. For the second approach, i.e. calculations of the cluster interactions, a series of results has been proposed by Carlsson, using Connolly–Williams inversion [28, 29] with a resummation scheme which leads to concentration dependent effective pair interaction (EPI). These so-obtained EPI are qualitatively comparable to the ones obtained from mean field methods based on multiple-scattering theory [30] and give very short-ranged interactions and strong ordering tendencies. A tight-binding approach based on the Cluster Bethe Lattice Method (CBLM) has also been used and gives EPI values very close to Carlsson's ones [22].

The purpose of this work is to present a complete calculation of the phase diagram of the binary NiAl system combining the tetrahedron approximation of the CVM and the linear muffin-tin orbital method (LMTO). This determination requires the knowledge of SRO in solid solutions based on BCC and FCC underlying lattices, the stability of the different compounds in the binary system and the liquid phase. The paper is organized as follows. In section 2, we present a brief review of the quantum and statistical mechanical approaches used in our calculations. In section 3, we present the results of our calculations and compare them with the experimental ones.

2. Free energy model

In order to compute a phase diagram, we need to know the total free energy of the binary alloy in a given phase, then its energy and also its entropy of formation.

For the alloy in phase α, the total free energy may be written as

$$F^{\alpha} = (1 - c)F_{\mathrm{A}}^{\alpha} + cF_{\mathrm{B}}^{\alpha} + E_{\mathrm{f}}^{\alpha} - TS_{\mathrm{f}}^{\alpha} \tag{1}$$

where c is the concentration of the B element, F_{I}^{α}, the free energy of pure element I in phase α, E_{f}^{α} and S_{f}^{α} are respectively the enthalpy and entropy of alloy formation.

The first simplifying assumption regarding the evaluation of this total free energy is to assume that the free energy for the pure elements can be written as

$$F_{\mathrm{I}}^{\alpha} = E_{\mathrm{I}}^{\alpha} - TS_{\mathrm{I}}^{\alpha} \tag{2}$$

in which the cohesive energy E_{I}^{α} and entropy S_{I}^{α} are both temperature independent.

The second assumption assumes that S_{f}^{α} is a purely configurational term, which means that the remaining entropy depends only on the concentration via the first two terms on the right hand side of (1).

2.1. Energy of formation

It has been shown in the introduction that to perform phase diagram calculations, the internal energy of an A–B alloy is assumed to be described in terms of a rapidly convergent series of concentration-independent multi-site interactions. More precisely, we assume that the total energy of a particular configuration α is expressed by [31]

$$E_{\mathrm{tot}}^{\alpha}(r) = \sum_{\gamma}^{\infty} V_{\gamma}(r)\xi_{\gamma}^{\alpha} \tag{3}$$

$V_{\gamma}(r)$ is the concentration–independent multi-site interaction associated with the multi-site correlation ξ_{γ}^{α} defined as [32]

$$\xi_{\gamma} = (1/N\gamma) \sum_{|n_j|} \sigma_{n_1}\sigma_{n_2} \ldots \sigma_{n_{\gamma}}$$

where $\sigma_n = 1 - 2p_n$, takes the values $+1$ or -1 depending on the occupancy of site n, $N\gamma$ is the total number of γ-type clusters, and the sum runs over all γ-type clusters that can be formed by combining sites on the entire crystal. The total energies and the multi-site interactions are generally lattice-parameter r (or volume) dependent.

Given (3), the interactions are determined by an inversion of the sum for a finite number of configurations defined by the existence of a maximum cluster $\gamma_{\max}$ beyond which the multi-site interactions vanish.

Hence, from a finite number of total energies for ordered structures and by truncating the summation in (3), a set of multi-site interactions is obtained from

$$\begin{aligned} V\gamma(r) &= \sum_{\alpha} (\xi_{\gamma}^{\alpha})^{-1} E_{\mathrm{f}}^{\alpha}(r) \qquad && \Phi < \gamma < \gamma_{\max} \\ V\gamma(r) &= 0 && \gamma_{\max} < \gamma < \infty \end{aligned} \tag{4}$$

Φ is the empty cluster.

Of course, one performs total energy calculations of as many ordered structures as there are unknown multi-site interactions required by the truncation but it is clear that, in this approach, this truncation leads to a non-uniqueness of the cluster interactions [32]. However, if the concentration-independent multi-site interactions decay rapidly, one can expect that this difficulty becomes minor and then in practice, the interactions can be uniquely computed.

In a series of papers, [28, 29, 33], Carlsson has computed cluster interactions for FCC and BCC alloys of aluminium with transition metals using Connolly–Williams inversion. For FCC calculations, he used A–FCC, B–FCC, A_3B–$L1_2$, AB_3–$L1_2$, and AB–$L1_0$ with ideal c/a ratio. Only first-nearest-neighbour pair interactions, triangle and tetrahedron cluster interactions are included. For BCC calculations, he takes A–BCC, B–BCC, A_3B–DO_3, AB_3–DO_3, AB–B2 and AB–B32. In this case, first- and second-nearest-neighbour pair interactions, triangle and tetrahedron cluster interactions are taken into account. He finds that this truncation is a reasonable approximation for these systems; for a Ni–Al system, the convergence of the cluster expansion appears to be very rapid, three- and four-atom terms having 15% and 5% of the magnitude of the pair terms [28]. This result is confirmed by the results for the effective pair interaction obtained via the Generalized Perturbation Method applied to the Korringa–Kohn–Rostoker multiple scattering formulation of the Coherent Potential Approximation (KKR-CPA) which finds roughly a factor of ten reduction at the second-neighbour distance [30].

Carlsson has also shown that it is possible to convert multi-site interactions into concentration dependent effective pair interactions [28]. They are obtained by making a truncated approximation in the higher-order correlation functions, using only the pair correlation function. Even if this development suffers from a loss of accuracy, the effective pair interactions present advantages in their ease of interpretability and their practical usefulness.

Then, using first-principles total energy calculations, we are able to compute the energies of formation of stoichiometric compounds occurring in the studied phase diagram and the multisite interactions allowing us to treat short-range order in the FCC- or BCC-based solid solutions or ordered superstructures presenting an extended concentration range.

2.2. *Configurational entropy*

As for the energies of formation, different configurational entropy approximations depending on the nature of the phase being considered are used. For the strictly stoichiometric compounds, the configurational entropy is taken equal to zero. For the solid solutions, or ordered phases presenting an extended concentration range, the configurational entropy is described by means of the CVM. The CVM entropy is found to be approximately given by a sum of the partial cluster entropies [34]. The maximum cluster used in our study is the tetrahedron containing first and second neighbours in the BCC lattice. In the tetrahedron approximation, the entropy of a BCC disordered system is given by [16]

$$S^{\mathrm{BCC}} = -k_{\mathrm{b}}\left(6\sum_{ijkl} w_{ijkl}\ln w_{ijkl} - 12\sum_{ijk} t_{ijk}\ln t_{ijk} + 3\sum_{ij} y_{ij}^{(2)}\ln y_{ij}^{(2)} + 4\sum_{ik} y_{ik}^{(1)}\ln y_{ik}^{(1)} + \sum_{i} x_i \ln x_i\right) \tag{5}$$

where $w_{ijkl}, t_{ijk}, y_{ij}^{(2)}, y_{ik}^{(1)}$ and x_i denote, respectively, the probability of finding tetrahedra, triangles, second-neighbour pairs, first-neighbour pairs and points in the configuration given by the subscripts (i equals A or B in a binary alloy).

For the disordered FCC structure we have

$$S^{FCC} = -k_b \left(2 \sum_{ijlk} w_{ijkl} \ln w_{ijkl} - 6 \sum_{ik} y_{ik}^{(1)} \ln y_{ik}^{(1)} + 5 \sum_{i} x_i \ln x_i \right). \tag{6}$$

The cluster probabilities are related by the following consistency relationships

$$t_{ijk} = \sum_{l} w_{ijkl} \tag{7a}$$

$$y_{ij}^{(2)} = \sum_{kl} w_{ijkl} \tag{7b}$$

$$y_{ik}^{(1)} = \sum_{jl} w_{ijkl} \tag{7c}$$

$$x_i = \sum_{jlk} w_{ijkl}. \tag{7d}$$

For the case of an ordered phase present in a range of concentration, long-range order is described in the usual manner by means of sublattices reflecting the symmetry of the ordered structure. A given cluster may now consist of points in the crystal belonging to different sublattices and their probabilities have to be distinguished accordingly (see [35] for more details).

2.3. Liquid alloys

Liquid alloys may also display SRO as has recently been shown for liquid $Al_{80}Ni_{20}$ alloy [36] and it is essential to consider SRO when determining the thermodynamic data. The best way to perform such calculations is to use a variational method with, as a reference system, a mixture of hard spheres which all have the same diameter but different charges and which interact through a screened Coulomb potential [37]. This reference system has been found, coupled with pseudo-potentials or TB–CBLM, to describe well the structural and thermodynamics manifestations of ordering in disordered alloys [38]. Very recently, it has been shown, using a tight-binding description of the total energy of the alloy [39] that, for the thermodynamic quantities, similar results are found for transition metal-based alloys if the liquid configurational free energy is approximated by the tetrahedron approximation of the CVM free energy in the disordered FCC structure. We have kept this approximation to describe the Ni–Al liquid phase in the present work.

2.4. Phase equilibrium

In order to determine the equilibrium phase diagram, it is more convenient to minimize the grand potential Ω given by

$$\Omega = F - \mu \xi_1 \tag{8}$$

where μ is the effective chemical potential. In the present work, the minimization of the grand potential is carried out with respect to a set of independent configurational variables and the variable r, since effective cluster interactions are also a function of the lattice parameter; in the use of the tetrahedron approximation, these configurational

variables are chosen to be the tetrahedron probabilities w_{ijkl} at constant temperature T and effective chemical potential μ, taking into account the normalization constraint

$$\sum_{ijlk} w_{ijkl} = 1. \tag{9}$$

This minimization is done using the Natural Iteration (NI) method developed by Kikuchi [40]. The NI equations used in the present model have been presented elsewhere [16] and will not be repeated here.

The equilibrium phase diagram between the two phases I and II is computed using the same scheme as proposed by Kikuchi and Murray [41]. For the same initial value of the effective chemical potential μ, the grand potentials of phases I (Ω_I) and II (Ω_{II}) are calculated using the procedure described above. If $\Omega_I = \Omega_{II}$, the equilibrium conditions are realized, but if not, the value of μ is modified until $\Omega_I = \Omega_{II}$.

3. Results for the Ni–Al system

The Ni–Al phase diagram displayed in figure 1 is characterized by a liquid phase, a FCC (A1) phase at both the Al and Ni rich ends, a non-congruently melting compound Al_3Ni and three intermediate phases with a variable range of solubilities Al_3Ni_2, AlNi and $AlNi_3$. Several attempts have been made to describe the NiAl phase diagram. As already mentioned, Sigli and Sanchez [16] have shown that the tetrahedron approximation of the CVM is an appropriate system to describe the phase diagram of this binary system.

In that case, EPI were determined from experimental thermodynamic data and available phase diagram information; these EPI are in good agreement with the ones determined by Carlsson [28] and Colinet *et al* [22] using quantum mechanics arguments.

3.1. Ground states at zero temperature

As a first step, we have calculated the energies of formation of the four intermediate phases observed in the equilibrium phase diagram. In the *structurbericht* notation, these phases are called the orthorhombic DO_{20} (Al_3Ni) phase, the hexagonal $D5_{13}$ (Al_3Ni_2) phase, the cubic B2(AlNi) phase and the cubic $L1_2$ ($AlNi_3$) phase. We have also selected two other FCC superstructures, $L1_2$(Al_3Ni) phase and $L1_0$(AlNi) phases and three other BCC superstructures, $D0_3$(Al_3Ni), $D0_3$($AlNi_3$) and B32(AlNi) phases. All these calculations allow us to check our prediction of the correct ground states and also to extract multi-site interactions to study the B2 (AlNi) and $L1_2$ ($AlNi_3$) phases, stable over an extended concentration range and described as SRO-phases. We mention that although the hexagonal $D5_{13}$ phase is experimentally reported to be stable over a small concentration range, it will be described as a stoichiometric compound.

To calculate the energies of the different phases, we have employed the all-electron total energy local density formalism as carried out with the linear muffin-tin orbital (LMTO) method [21]. The LMTO calculations have been done in the atomic sphere approximation, including combined corrections, as developed in the code of M van Schilfgaarde, A T Paxton and M Methfessel (unpublished result). We have used the parametrization of the von Barth Hedin exchange correlation energy density given by Moruzzi *et al* [42]. In our Brillouin zone integrals, we use a uniform mesh of sampling points with at least 16 divisions along each of the primitive vectors. With such a mesh, we obtain a convergence of the absolute value of the total energy of 0.1 mRy. The same

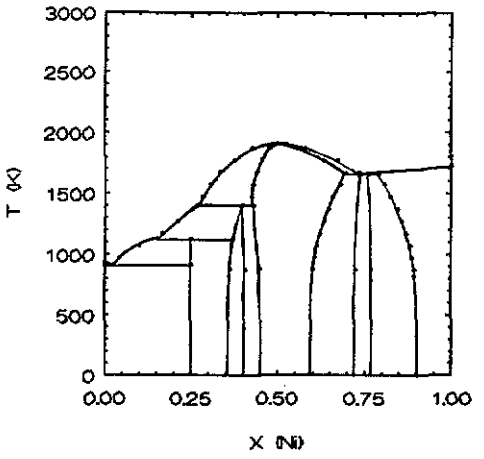

Figure 1. Experimental phase diagram of the Ni–Al system.

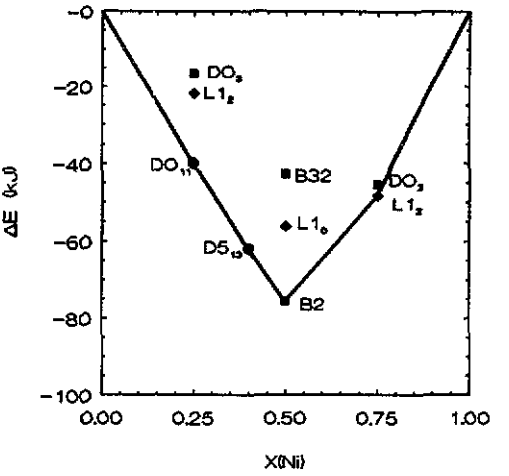

Figure 2. Formation energies as a function of composition for all the compounds studied.

Table 1. LMTO results for cohesive energies and equilibrium molar volumes of different structures in the Ni–Al system.

Structure		Composition	Cohesive energy (kJ mol^{-1})	Lattice parameter (au)
FCC	A_1	Ni	−584.231	6.52
	$L1_2$	Ni_3Al	−586.732	6.675
	DO_{22}	Ni_3Al	−584.074	6.685
	$L1_0$	NiAl	−548.698	6.828
	$L1_2$	$NiAl_3$	−468.407	7.185
	DO_{22}	$NiAl_3$	−469.580	7.146
	A_1	Al	−400.794	7.522
BCC	A2	Ni	−581.185	5.188
	DO_3	Ni_3Al	−585.104	5.270
	B2	NiAl	−568.112	5.413
	B32	NiAl	−535.162	5.426
	DO_3	$NiAl_3$	−463.064	5.674
	A_2	Al	−395.569	6.003
	$D5_{13}$	Ni_2Al_3	−536.019	7.500
	DO_{20}	$NiAl_3$	−486.543	12.350

radius value was taken for the Wigner–Seitz spheres of all the elements and we include the spherical harmonic up to $l = 2$ (d orbitals) in constructing the basis functions.

For each structure, the total energies provided by the LMTO method are obtained for different values of the volume, the minimum of this curve determined the equilibrium total energy and the equilibrium volume. Moreover, the bulk modulus, which is related to the curvature of the total energy with volume is obtained using a fit based on Murnaghan's equation of state [43]. In table 1, are calculated equilibrium cohesive energies and molar volumes of all the considered phases. We recall that the cohesive

energy is defined as the difference of the total energy of that phase and the total energy of the constituent atoms at infinite interatomic distances. The ground states of both Ni and Al are predicted to be FCC. The energy difference between the FCC and BCC structures, defined as $\Delta E_{\text{FCC-BCC}} = E_{\text{coh}}^{\text{FCC}} - E_{\text{coh}}^{\text{BCC}}$, is 3.046 kJ mol^{-1} and 5.224 kJ mol^{-1} for Ni and Al respectively. We mention that the value of the structural energy difference for Al is very close to the one obtained by FLAPW calculations [15]. Figure 2 shows results for the formation energies as a function of composition for all the studied compounds. These formation energies are defined as

$$\Delta E = E_{\text{coh}} - x_{\text{Ni}} E_{\text{coh}}^{\text{FCC}}(\text{Ni}) - x_{\text{Al}} E_{\text{coh}}^{\text{FCC}}(\text{Al}). \tag{10}$$

At the equiatomic composition, the calculated formation energies of the competing phases, i.e. B2, B32 and $L1_0$ phases, strongly favour the B2 phase in complete agreement with experimental data. The computed value for ΔE of -75.6 kJ mol^{-1} is more negative than the experimental value, -58.8 kJ mol^{-1} [27]. However, our result is in complete agreement with other theoretical determinations [17] but this phase is known to present anti-sites and vacancies even at the equiatomic composition, factors which are not considered in these calculations. For 75% of Ni, the $L1_2$ phase is predicted to be more stable than the DO_3 phase, both being more stable with regard to a mixture of the Ni–FCC and NiAl–B2 phase. The computed value for ΔE of -48.36 kJ mol^{-1} compares well with the experimental value, -41.0 kJ mol^{-1}. For 25% of Ni, the $L1_2$ phase is found to be yet more stable than the DO_3 phase, but its value is located well above the line connecting the formation energies of Al–FCC and NiAl–B2 phases. In fact for this composition, the most stable structure is the DO_{20} orthorhombic phase, a result which is also obtained in our calculations. Its calculated formation energy, -39.89 kJ mol^{-1} is in complete agreement with the experimental value, -37.7 kJ mol^{-1}.

At 40% of Ni for which the hexagonal $D5_{13}$ phase is experimentally reported to be stable over a small concentration range, there is no superstructure based on the BCC or FCC lattice. However, it is predicted to be more stable with regard to a mixture of $NiAl_3$–DO_{20} and NiAl–B2 phases since the calculated formation energy, -61.85 kJ atom^{-1}, close to the experimental one, -56.5 kJ atom^{-1}, is just above the line connecting the formation energies of both DO_{20} and B2 phases.

3.2. Cluster interactions and disordered alloys

As already mentioned, the concentration-independent multi-site interactions can be extracted from the total energy calculations using the Connolly–Williams inversion method.

In figures 3(*a*) and (*b*) are presented cluster interactions obtained for the FCC and BCC lattices as a function of the volume. These results reveal a very small difference between the FCC and BCC interaction parameters. V_0 and V_1 display a strong volume dependence. The shape of V_0 is similar to the one of the $E(V)$ function since V_0 is given by a sum of the energies of the different superstructures occurring on a given lattice. The shape of V_1 is essentially due to the fact that the two alloying elements present two different volumes. Let us mention that the strengths of V_3 and V_4 are much smaller than that of V_2, indicating a reasonable degree of convergence already at the four atom supercell level. At this level of discussion we recall that in the tetrahedron approximation of the Connolly–Williams method for FCC-based structures, the $L1_2$ and DO_{22} structures display the same correlations and then are degenerate. LMTO results provide that for $x_{\text{Ni}} = 0.25$, $E_{L1_2} - E_{DO_{22}} = +1.17$ kJ mol^{-1} while for $x_{\text{Ni}} = 0.75$, $E_{L1_2} - E_{DO_{22}} =$

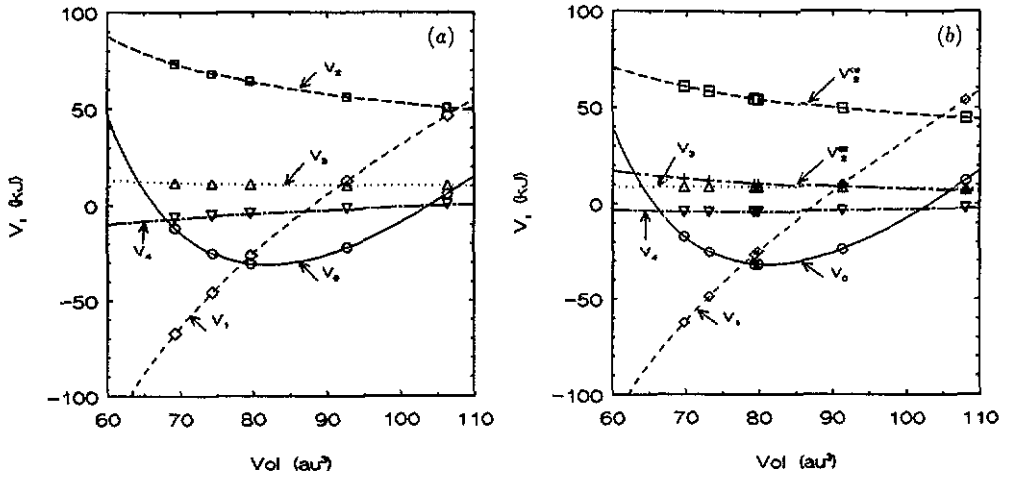

Figure 3. Cluster interactions as a function of the volume (*a*) FCC lattice; (*b*) BCC lattice.

-2.66 kJ mol^{-1}. These two differences are small indicating also that the tetrahedron approximation is reasonable. It is interesting to compare the results obtained by LMTO calculations to the ones provided by GPM-KKR-CPA [30] or TB-CBLM [22] approaches. This can be done by calculating the disordered energy and the effective pair interactions as a function of composition.

The disordered energy is obtained using the fact that the pair and higher order correlations are given as products of the point correlations for the totally disordered state. For the FCC and BCC-based structures, all atomic positions are equivalent and we have:

$$\xi_\gamma^{\text{dis}} = (\xi_1)^n\gamma \tag{11}$$

where n_γ is the number of sites contained in the γ cluster. The energy of the disordered configuration is then given by

$$E_{\text{tot}}^{\text{dis}} = \sum_{\gamma}^{\gamma_{\max}} V\gamma(\xi_1)^n\gamma. \tag{12}$$

Comparing cluster interactions from the CVM and effective pair interactions from GPM or CBLM can be done using a resummation of the higher order cluster interactions at fixed concentration, corresponding to a lowest order expansion of the total energy in powers of the short-range parameters [28].

With the set of clusters used in our calculations, we obtain for the FCC lattice

$$V_2^{\text{eff}} = \tfrac{1}{6}(V_2 + 3V_3\xi_1 + 6V_4\xi_1^2) \tag{13}$$

and for the BCC lattice:

$$\begin{aligned} V_2^{(1)\text{eff}} &= \tfrac{1}{4}(V_2^{(1)} + 2V_3\xi_1 + 4V_4\xi_1^2) \\ V_2^{(2)\text{eff}} &= \tfrac{1}{8}(V_2^{(2)} + V_3\xi_1 + 2V_4\xi_1^2) \end{aligned} \tag{14}$$

where the effective pair interactions V_2^{eff} are defined as

$$V_2^{\text{eff}} = \tfrac{1}{4}(V_{\text{AA}} + V_{\text{BB}} - 2V_{\text{AB}}) \tag{15}$$

V_{AA}, V_{BB}, V_{AB} are pair potentials evaluated at the separation between first-nearest

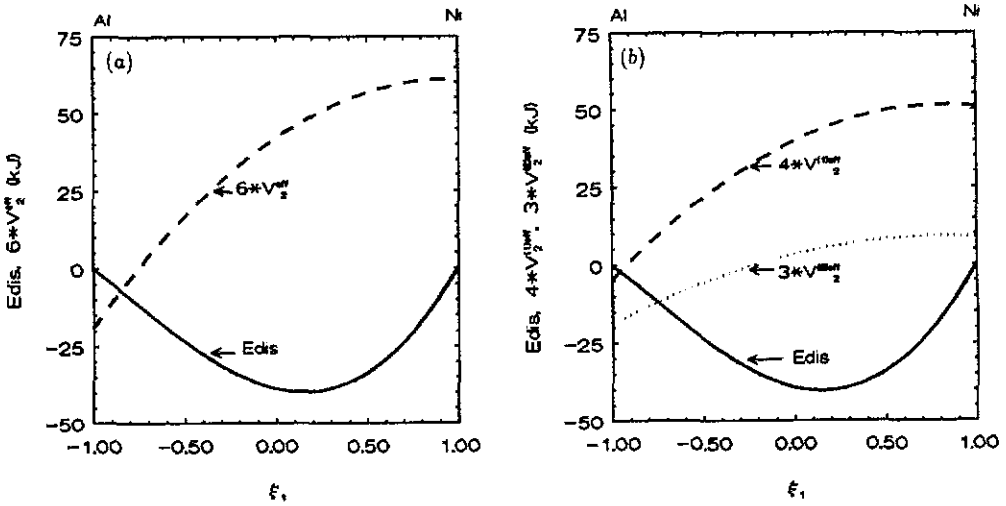

Figure 4. Concentration-dependent effective pair interactions and random energies (*a*) FCC lattice; (*b*) BCC lattice.

neighbours for the FCC lattice and first- and second-nearest neighbours for the BCC lattice.

As already mentioned by Carlsson, the EPI dependence as a function of the concentration is given by a higher order cluster than the pair here, triangle and tetrahedron. Two distinct approaches are used to obtain the concentration-dependent EPI: (i) the 'locally relaxed' treatment for which each cluster in the alloy is able to relax to its preferred lattice constant; (ii) the 'frozen lattice' treatment where each cluster is calculated at a fixed lattice constant. We use the 'locally relaxed' treatment of the lattice relaxation effects, which is considered to be more accurate than the 'frozen lattice' treatment [28]. In figure 4 are displayed values for the first-nearest-neighbour interactions on the FCC lattice as a function of ξ_1 (with ξ_1 equal to x_{Ni}–x_{Al}). Our results are of course very similar to Carlsson's ones since the augmented-spherical wave (ASW) and LMTO methods used to calculate total energies are essentially the same. Tight-binding based results present the same concentration dependence [22], and a large positive value of V_2^{eff} at the Ni rich end, consistent with the very strong ordering tendency in Ni_3Al which remains ordered up to its melting point; at the Al-rich end, the value of V_2^{eff} drops rapidly.

Our calculated EPI also display a semiquantitative agreement with tight-binding ones, $V_{FCC}^{(2)eff}$ being equal to 2.84 kJ, 7.02 kJ and 10.34 kJ for $x_{Ni} = 0.25$, 0.5 and 0.75, respectively, while they are equal to 2.65 kJ, 4.58 kJ and 7.0 kJ in Colinet's approach. Another instructive comparison can be done with EPI determined by Turchi *et al* [30] in Ni–Al alloys around an equiatomic composition. These authors found $V_2^{(1)eff}$ (BCC) = 8.20 kJ for $x_{Ni} = 0.5$ compared to 9.97 kJ extracted from LMTO calculations or to 6.75 kJ obtained by Colinet *et al* [22].

In fact, Carlsson's resummation procedure corresponds to a high temperature expansion of the correlation functions and may be considered to be a good approximation to describe effective pair interactions in the liquid phase. For this kind of liquid alloy, experimental results based on neutron diffraction experiments [36, 44] have shown that

A–A and B–B distances are quite similar in the alloys but different from the nearest distances in pure liquids. Moreover it has been found that the local coordination is roughly equal to 11, very close to the FCC-coordination. Then, for each concentration, E_{dis} and V_2^{eff} used to describe the liquid part are obtained from (12), (13) at a fixed given volume. However, for each concentration a new volume is used. The concentration-dependent volume is taken to be similar to the one obtained for the FCC-based solid solution which displays a similar variation to the experimental one seen in the liquid phase [45]. Another argument to justify this approximation is that if the pair interactions of the FCC and BCC lattices come out similarly, then they are not sensitive to the underlying lattice (at least for the Ni–Al system).

In figure 5 are plotted these values of the V_2^{eff} as a function of the concentration. By comparison with the EPI obtained by the 'locally' relaxed treatment on the FCC and BCC lattice, we can see that these new values of V_2^{eff} display a smoother variation as a function of the composition.

The same conclusion is reached from the comparison of the random energy obtained in the locally relaxed treatment for the FCC and BCC lattices with the values obtained by this new treatment. From figures 4 and 5, we see that the three curves display negative values at all concentrations; the minimum is shifted towards the Ni rich part for the two curves obtained by the 'locally relaxed' treatment. The third curve displayed in figure 5, and used to describe the liquid phase, presents a more symmetrical shape.

3.3. Phase diagram calculations

Let us sum up the strategy of our calculations.

(i) The energies of the four compounds occurring in the phase diagram are obtained as a function of the volume. The minima of these curves are chosen to obtain the formation energies of these compounds. The entropies are considered to be equal to zero for the strictly stoichiometric compounds such as Al_3Ni, Al_3Ni_2 phases. For AlNi and $AlNi_3$ phases, the entropies of configuration will be given by the tetrahedron approximation of the CVM for ordered phases based on the FCC or BCC lattices.

(ii) The two solid solutions based on the FCC and BCC lattices are described as short-range-order solutions using the CVM treatment in its tetrahedron approximation. The cluster interactions are obtained as a function of the volume using the Connolly–Williams approach.

(iii) The difference in energy between FCC and BCC structures are taken from LMTO results.

(iv) The liquid phase is also described as a short-range-order phase using the tetrahedron approximation of the CVM free energy in the disordered FCC structure. The effective pair interactions are obtained from Carlsson's resummation procedure which corresponds to a high temperature expansion of the correlation functions. Although this model is developed with a solid-state approximation, it does a good job of describing the influence of chemical short-range order on the thermodynamic properties of the liquids [39, 46]. Of course, the continuous phase space of the nucleii's motion and structural information, such as pair correlation functions, are lost. However, the chemical ordering contribution to the entropy and the energy, which are quantities of central interest in our calculations, are only proportional to the concentration fluctuations. Using a statistical approach based on a 'discretized mesh' rather than the continuous

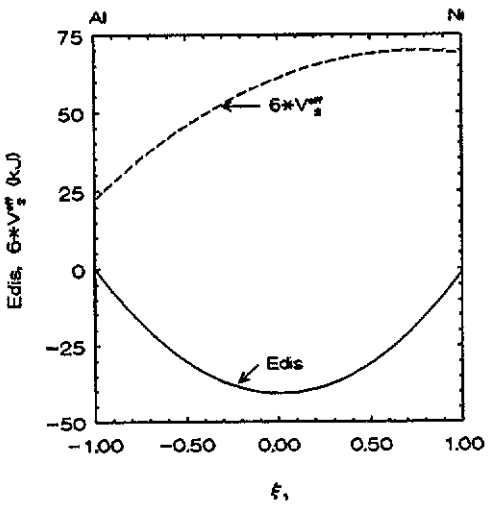

Figure 5. Concentration-dependent effective pair interactions and random energy for liquid phase.

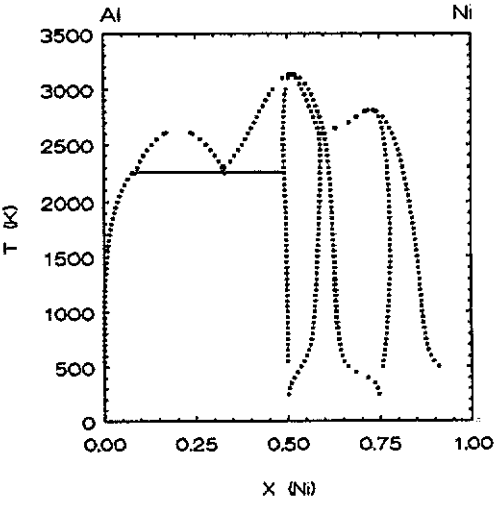

Figure 6. The Ni–Al phase diagram calculated with only FCC-based structures taken into account.

phase space of the nucleii's motion may be considered as correct to describe the concentration fluctuations.

However, there is still a 'missing link' in our approach which is the thermodynamic properties of the pure metals or, in other terms, the difference in free energy between the liquid and crystalline phases. Although the density functional theory has made significant progress in the modelling of liquids, application to the determination of the melting temperatures does not yet appear possible. Therefore, we have chosen to use thermodynamic compilations to obtain melting temperatures $T_l^{FCC\to liq}$ and the latent heat of melting $\Delta E_l^{FCC\to liq}$ for both Ni and Al elements [47]. In this case the free energy of these elements in their liquid state is given by

$$F_l^{liq}(T) = E_l^{FCC} + \Delta E_l^{FCC\to liq} - T(\Delta E^{FCC\to liq})/(T_l^{FCC\to liq}). \tag{16}$$

If only FCC-based equilibria are considered, the phase diagram of figure 6 is produced. Of course, only the Ni-rich portion can be directly compared with experimental results since for Ni concentration less than 0.75 structures other than FCC-based superstructures appear. The main features of the diagram are a miscibility gap (MG) with a maximum temperature of 2630 K and two ordered phases $L1_2$ and $L1_0$ with transition temperatures of 2820 and 3135 K respectively. As already mentioned by Carlsson and Sanchez [48], the MG is caused by an elastic instability and can be understood through the concentration dependence of the calculated energy of mixing for the completely random FCC solid solution. ΔE_{rand} is negative at all concentrations like the curves obtained with the 'locally relaxed' treatment (see figure 4) but here its curvature is negative for Ni concentrations less than 30%: this curvature is due to the peculiar volume dependence of V_2, V_3 and V_4, and another way to come to the same conclusion is to compute the phase diagram ignoring volume effects altogether. In that case the diagram displayed in figure 7 strongly resembles the previous diagram except for the MG on the Al-rich side.

When the families of both FCC and BCC-based free energy curves are combined with the stoichiometric Al_3Ni and Al_3Ni_2 compounds and the liquid phase, the phase diagram of figure 8 is obtained. All the main features of the experimental phase diagram (see

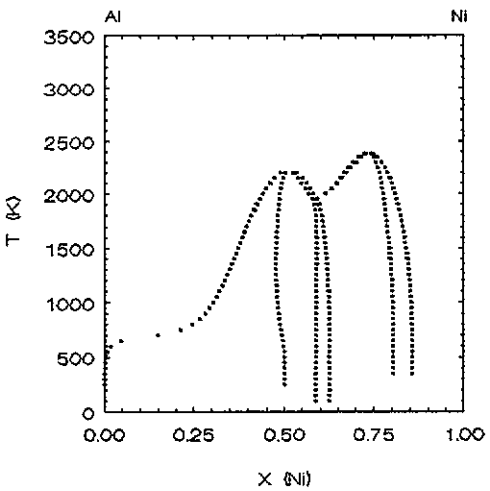

Figure 7. As figure 6 but now without including the volume dependence of the cluster interactions.

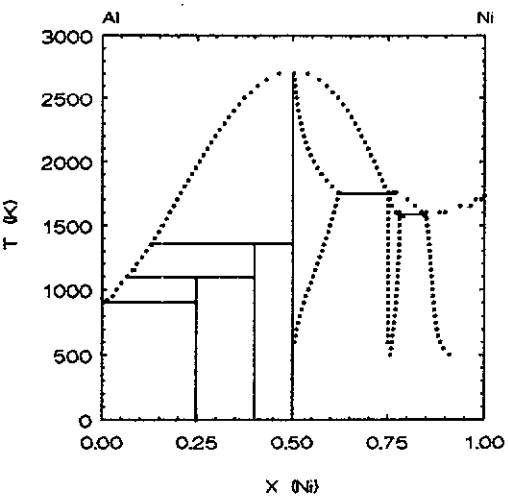

Figure 8. Calculated phase diagram of the Ni–Al system.

figure 1) have, at least qualitatively, been reproduced. The quantitative agreement is not as good.

(i) The B2 phase is found to melt congruently at $T = 2600$ K, before undergoing a disordering reaction. Its overestimate of the melting temperature seems to be attributable to the overestimate of the heat of formation of the B2 compound. However, in a more recent paper [49] Desai gives an experimental value of the heat of formation of the NiAl compound equal to -71.65 kJ mol^{-1} which is very close to our calculated value. He mentions the difference between the experimental values but no explanation is provided. Then the origin of the discrepancy of the calculated phase diagram with the experimental phase diagram in this region is not clear. Let us recall that this compound is known to present antisites and vacancies even at the equiatomic composition, factors which are not considered in these calculations.

(ii) The computed phase diagram exhibits two eutectics, one at the Al-rich side and another at the Ni-rich side, just like the experimental phase diagram. The calculated eutectic temperatures are in relatively good agreement with the experimental ones since they have been found equal to 900 K at the Al-rich side and 1680 K at the Ni-rich side (compared with 913 K and 1658 K respectively).

(iii) The two complex DO_{20} and $D5_{13}$ structures are found to melt peritectically. For the Al_3Ni compound, the peritectic temperature is some 27 K lower than experiment indicates but for the Al_3Ni_2 compound it is 56 K higher than the experimental one.

Our calculations lead also to a peritectic decomposition of the Ni_3Al compound. More particularly, the eutectic between the solid phase A_1, $Ni_3Al(L1_2)$ and the liquid one takes place on the right of the peritectic, which is in agreement with the usually adopted phases diagrams. However, let us mention that this part of the phase diagram is very sensitive to the values of the energies of the three phases which determine the equilibrium properties. From an experimental point of view, we point out that the phases boundaries of the peritectic decomposition of the Ni_3Al compound are still controversial.

4. Conclusion

It was shown that *ab initio* calculations of the Ni–Al phase diagram are, in many points, in agreement with experimental information. They have been obtained by combining total energy LMTO calculations with the tetrahedron CVM approximation. No relaxation and no vibrational effects have been taken into account. Only short-range order on FCC and BCC lattices have been introduced using CVM treatment in competition with the occurrence of complex phases like the DO_{20} and $D5_{13}$ phases. The thermodynamic description of the liquid phase has been achieved by approximating this phase to a FCC-based disordered phase to minimize the number of parameters. The melting temperature and latent heat of the pure components are the only two parameters which have been introduced from outside the first-principles matrix. We believe that our results show that first-principles studies of phase equilibria may now be considered as feasible with a good degree of confidence.

Acknowledgment

ATP and MVS acknowledge financial support under AFSOR contract F49620-88-K-0009.

References

[1] For a review, see Srivastatva G P and Weaire D 1987 *Adv. Phys.* **36** 463
[2] Kikuchi R 1951 *Phys. Rev.* B **81** 988
[3] Binder K 1986 *Monte Carlo Methods in Statistical Physics (Springer Series on Topics in Current Physics 7)* ed K Binder (Berlin: Springer)
[4] Velicky B, Kirkpatrick S and Ehrenreich H 1968 *Phys. Rev.* **175** 747
[5] Gonis A, Zhang X A, Freeman A J, Turchi P, Stocks G M and Nicholson D M 1987 *Phys. Rev.* B **36** 4630
[6] Ducastelle F and Gautier F 1976 *J. Phys. F: Met. Phys.* **6** 2039
[7] Turchi P, Stocks G M, Butler W H, Nicholson D M and Gonis A 1988 *Phys. Rev.* B **37** 5982
[8] Sigli C, Kosugi M and Sanchez J M 1986 *Phys. Rev. Lett.* **57** 253
[9] Sluiter M, Turchi P, Zchong Fu and De Fontaine D 1988 *Phys. Rev. Lett.* **60** 716
[10] Le D H, Colinet C, Hicter P and Pasturel A 1991 *J. Phys.: Condens. Matter* **3** 7895
[11] Connolly J W D and Williams A R 1983 *Phys. Rev.* B **27** 5169
[12] Ferreira L G, Mbaye A A and Zunger A 1987 *Phys. Rev.* B **35** 6475
[13] Zunger A, Wei S H, Mbaye A A and Ferreira L G 1988 *Acta Metall.* **36** 2239
[14] Mohri T, Terakura K, Oguchi T and Watanabe K 1988 *Acta Metall.* **36** 547
[15] Sluiter M, de Fontaine D, Guo X Q, Podłoucky R and Freeman A J 1990 *Phys. Rev.* B **42** 10460
[16] Sigli C and Sanchez J M 1985 *Acta Metall.* **33** 1097
[17] Hackenbracht D and Kübler J 1980 *J. Phys. F: Met. Phys.* **10** 427
[18] Xu J H, Oguchi T and Freeman A J 1987 *Phys. Rev.* B **36** 4186
[19] Sarma D D, Speier W, Zeller R, Van Leuken E, de Groot R A and Fuggle J C 1989 *J. Phys.: Condens. Matter* **1** 9131
[20] Hong T and Freemand A J 1991 *Phys. Rev.* B **43** 6446
[21] Andersen O K 1984 *NATO ASI on Electronic Structure of Complex Systems* ed P Phariseau and W T Temmerman (New York: Plenum) p 11
[22] Colinet C, Bessoud A and Pasturel A 1989 *J. Phys.: Condens. Matter* **1** 5837
[23] van Schilfgaarde M, Paxton A T, Pasturel A and Methfessel M 1991 *MRS Spring Meeting 1990* vol 186 ed G M Stocks, A F Giamei and D P Pope (Pittsburgh, PA: Materials Research Society) p 107
[24] Pettifor D G 1978 *J. Chem. Phys.* **69** 2930
[25] Andersen O K, Skriver H L, Nohl H and Johansson B 1980 *Pure Appl. Chem.* **52** 93
[26] Harris J 1985 *Phys. Rev.* B **31** 1770
Foulkes W M C and Haydock R 1989 *Phys. Rev.* B **39** 12520

[27] Hultgren H, Desai P D, Hawkins D R, Gleiser M and Kelley K K 1973 *Selected Values of the Thermodynamic Properties of Binary Alloys* (Metals Park, OH: American Society for Metals)
[28] Carlsson A E 1987 *Phys. Rev.* B **35** 4858
[29] —— 1987 High Temperature Ordered Intermetallic Alloys *Proc. Symp. Materials Research Society (Boston, 1986)* vol 81, ed N S Stoloff, C C Koch, C T Liu and O Izumi (Pittsburgh, PA: Materials Research Society) p 39
[30] Turchi P, Sluiter M, Pinski F J and Johnson D D 1991 *MRS Spring Meeting 1990* vol 186 ed G M Stocks, A F Giamei and D P Pope (Pittsburgh, PA: Materials Research Society) p 59
[31] Mohri T, Sanchez J M and de Fontaine D 1985 *Acta Metall.* **33** 1171
[32] Sluiter M and Turchi P 1989 *Phys. Rev.* B **40** 11215
[33] Carlsson A E 1989 *Phys. Rev.* B **40** 912
[34] Kikuchi R and Sato H 1974 *Acta Metall.* **11** 1099
[35] Kikuchi R and de Fontaine D 1978 *Nation. Bureau of Standards, Report* No SP 496, p 967
[36] Maret M, Pomme T, Pasturel A and Chieux P 1990 *Phys. Rev.* B **42** 1598
[37] Pasturel A, Hafner J and Hicter P 1985 *Phys. Rev.* B **32** 5009
[38] Pasturel A and Hafner J 1986 *Phys. Rev.* B **34** 8357
[39] Pasturel A 1989 unpublished results
[40] Kikuchi R 1974 *J. Chem. Phys.* **60** 1071
[41] Kikuchi R and Murray J 1985 *Calphad* **9** 311
[42] Moruzzi V L, Janak J F and Williams A R 1978 *Calculated Electronic Properties of Metals* (New York: Pergamon) p 2
[43] Murnaghan F D 1944 *Proc. Natl. Acad. Sci. USA* **30** 244
[44] Maret M, Chieux P, Dubois J M and Pasturel A 1991 *J. Phys.: Condens. Matter* **3** 2801
[45] Ayushina G D, Levin E S and Geled P V 1969 *Russian J. Phys. Chem.* **43** 11
[46] Franz J R, Brouers F and Holzhey C 1980 *J. Phys. F: Met. Phys.* **10** 235
[47] Dindsdale A T 1988 *National Physical Laboratory Report*
[48] Carlsson A E and Sanchez J M 1988 *Solid State Commun.* **65** 527
[49] Desai P D 1987 *J. Phys. Chem. Ref. Data* **16** 109